Hindawi Publishing Corporation
Journal of Materials
Volume 2014, Article ID 235638, 8 pages
http://dx.doi.org/10.1155/2014/235638

Research Article

Synthesis and Characterization of Aluminum Doped Zinc Oxide Nanostructures via Hydrothermal Route

A. Alkahlout,[1,2] N. Al Dahoudi,[1,2] I. Grobelsek,[1] M. Jilavi,[1] and P. W. de Oliveira[1]

[1] *Leibniz-Institut für Neue Materialien (INM), Im Stadtwald, Gebaeude 22, 66123 Saarbruecken, Germany*
[2] *Department of Physics, Al-Azhar University-Gaza (AUG), P.O. Box 1277, Gaza Strip, Palestine*

Correspondence should be addressed to A. Alkahlout; dramalkahlout@yahoo.com

Received 4 December 2013; Accepted 6 February 2014; Published 25 March 2014

Academic Editor: Nelson Tansu

Stable crystalline aluminum doped zinc oxide (AZO) nanopowders were synthesized using hydrothermal treatment processing. Three different aluminum precursors have been used. The Al-precursors were found to affect the morphology of the obtained nanopowders. AZO nanoparticles based on zinc acetate and aluminum nitrate have been prepared with different Al/Zn molar ratios. XRD investigations revealed that all the obtained powders have single phase zincite structure with purity of about 99%. The effect of aluminum doping ratio in AZO nanoparticles (based on Al-nitrate precursor) on structure, phase composition, and particle size has been investigated. The incorporation of Al in ZnO was confirmed by UV-Vis spectroscopy revealing a blue shift due to Burstein-Moss effect.

1. Introduction

Zinc oxide ZnO is a wide band gap (3.4 eV) semiconductor which has broad range of potential uses in optical and electrical applications such as in solar energy conversion, thin film transistors, photocatalysis, nonlinear optics, gas sensors, pigments, cosmetic, LED, anti-UV and low-emission coatings, and photoluminescent and sensor materials [1–8].

Undoped ZnO shows n-type conductivity due to the existence of native defects such as oxygen vacancy, zinc interstitials, and hydrogen interstitials in the ZnO lattice [9–11]. Unfortunately, the conductivity of undoped ZnO is thermally unstable. The substitution of Zn^{2+} ions with group III ions (B^{3+}, Al^{3+}, Ga^{3+}, and In^{3+}) [8–16] generates extra electrons and improves ZnO optical, electrical, thermal, and magnetic properties. Al^{3+} has been the most used dopant element due to its small ionic radius and low material cost. The substitution of Zn^{2+} ions with Al^{3+} in ZnO lattice improves the electrical conductivity through the increase of charge carriers where it is reported that the electron concentration increases from 10^{16} to $10^{21}/cm^{-3}$ [17, 18]. The mobility of the charge carriers is strongly influenced by scattering at the disorder locations created in the crystal structure due to doping. Therefore, well crystalline doped ZnO particles, pure in phase, are very important for obtaining good electrical conducting properties. Accordingly, structural considerations should also be included [19].

The choice of aluminum precursor used for substitution of Al^{3+} ions in ZnO host lattice is very important. Organic salts are recommended for successful homogenous substitution [20]. On the other hand, doping based on aluminum's inorganic salts is reported to be not successful [21, 22].

In this work, AZO nanoparticles were synthesized using hydrothermal processing using different aluminum precursors and different aluminum doping concentrations. The obtained nanopowders were characterized using X-ray diffraction, electron microscopy, and UV-Vis spectroscopy.

2. Experimental Work

2.1. Preparation of AZO Nanoparticles (Different Al-Precursors). AZO nanoparticles were prepared starting with zinc acetate dihydrate $Zn(CH_3COO)_2{\cdot}2H_2O$ as zinc precursor and 3 different aluminum precursors typically: Al-chloride $AlCl_3$, Al-nitrate $Al(NO_3)_3$, and Al-isopropoxide $Al(O\text{-}i\text{-}Pr)_3$. The sol molarity was 0.5 M/L and Al/Zn = 1 mol.%. The synthesis method depended on the aluminum precursor as follows.

2.1.1. AZO Nanoparticles with Al-Chloride as Al-Precursor. 0.0667 g of Al-chloride was dissolved in 20 mL methanol under nitrogen. 10.9 g of zinc acetate dehydrate was dissolved in 80 mL of methanol at room temperature and added to Al-chloride sol where clear transparent sol was obtained. 3 M/L Na(OH) aqueous solution was added dropwise to the sol to get white precipitate. The pH value was adjusted to 11-12. The white colloid was left under stirring at room temperature overnight. It was treated hydrothermally for 12 h at 200°C. The precipitate was then washed with water 3-4 times and then dried in air at 100°C for 24 hours.

2.1.2. AZO Nanoparticles with Al-Nitrate as Al-Precursor. 10.9 g of zinc acetate dehydrate was dissolved in 80 mL of methanol at room temperature. The sol was left under stirring until clear sol is obtained. 0.187 g of Al-nitrate was dissolved in 20 mL of methanol and then added to zinc acetate sol and left under stirring for few hours. 3 M/L Na(OH) aqueous solution was added dropwise to the sol to get white precipitate. The pH value was adjusted to 11-12. The white colloid was left under stirring at room temperature overnight. It was treated hydrothermally for 12 h at 200°C. The precipitate was then washed with water 3-4 times and then dried in air at 100°C for 24 hours. For investigating the effect of Al-doping ratio, three different molar ratios were prepared, namely, 0.5, 1, and 2 mol.%.

2.1.3. AZO Nanoparticles with Al-Isopropoxide as Al-Precursor. The same steps followed in preparing AZO with Al-nitrate as precursor were repeated but Al-isopropoxide was used as aluminum precursor dissolving 0.12 g of Al-isopropoxide in 20 mL of methanol instead of 0.187 g of Al-nitrate.

2.2. Powder Characterization. Thermal properties of the powder have been determined by differential thermal analysis and thermal gravimetry analysis (DTA/TG) using a Netzsch STA 449 C Jupiter instrument. The AZO particles were dried in air at 100°C for 12 h and then grounded in a mortar to get a fine powder. 62.7 mg of the powder was heated in synthetic air in an Al_2O_3 crucible up to 500°C at a heating rate of 2 K/min.

The Brunauer-Emmett-Teller (BET) gas adsorption measurement technique was used to measure the surface area of the powders. The powder degassing was achieved using Autosorb Degasser station, and the measurements were conducted at liquid nitrogen saturation vapor pressure using Autosorb-6B from Quantachrome.

Powder X-ray diffraction (XRD) patterns of the samples were collected on a Bruker AXS D8 powder diffractometer unit, using Cu Kα radiation ($\lambda = 0.154$ nm), operating at 40 kV and 40 mA. A position sensitive detector (LynxEye) based on Bruker AXS compound silicon strip technology was used. The ZnO powders were scanned between $2\theta = 10^\circ$ and 100° with a 2θ scan step size of 0.005°. Glass sample holders were used as a support for all powder samples. The structural refinement of the obtained phases and profile analysis of the related diffraction patterns were carried out with the program TOPAS (general profile and structure analysis software for powder diffraction data, Bruker Analytical X-ray Systems). The mean crystallite sizes were calculated using the Scherrer equation (Scherrer constant $k = 1$). The integral breadth-based volume weighted calculation (of crystallite sizes) assuming intermediate crystallite size broadening of the peaks was modeled by a Voigt function.

The morphology of the AZO powder was evaluated by field emission scanning electron microscopy using a JEOL JSM 7500F instrument. The micrographs were taken at an accelerating voltage of 15 kV.

Transmission of powder dispersed in ethanol was measured using UV-VIS spectrometer (CARY 5000 from Varian). The measurements were carried out in UV range 300–3000 nm.

3. Results and Discussions

3.1. Effect of Al-Precursor

3.1.1. Phase and Structural Characterization (XRD). XRD patterns of powders grown under different manufacturing conditions did not show significant variations, except traces of additional phases (<10 wt%). The XRD pattern of ZnO phase was in agreement with published pdf data number 01-070-2551 (ICDD 2009) for synthetic zincite. It is known that under ambient conditions the thermodynamically stable phase of zinc oxide is zincite that crystallizes in the hexagonal *wurtzite* (ZnS, space group $P6_3mc$) structure. Figure 1 shows XRD patterns of aluminum doped zinc oxide AZO powder synthesised hydrothermally using Zn-acetate dihydrate and 3 different aluminum precursors, namely, Al-isopropoxide, Al-chloride, and Al-nitrate as doping starting materials. All samples have the Al/Zn doping ratio of 1 mol.%. Powder prepared with Al-isopropoxide favours the formation of single phase zincite structure while powder synthesised using Al-chloride and Al-nitrate contains traces of additional phases (see Table 1). Due to the low intensity, these traces could not be reliably identified. Pure zincite structure for such samples is obtained by heating the powder at 400°C in air for 30 min.

It is found that the intensity ratio of (101/002) peaks of AZO powder, prepared using Al-chloride precursor, is considerably high compared with that of other samples. It is considered that the variation of the (100)/(002) intensity ratio is influenced by the shear stress on the particles when it is compacted in the XRD holder.

3.1.2. Morphological Characterization (SEM). Figure 2 shows the SEM photographs of AZO particles prepared hydrothermally from the solution of zinc acetate dihydrate and three different Al-precursors. It is evident that the starting chemicals used for the synthesis of AZO nanoparticles have a strong influence on the morphology of the obtained powders. As seen in Figure 2(a), using zinc acetate dihydrate and Al-chloride results in formation of large agglomerates having hexagonal rod-like shape with a tip (see inset). The length of the agglomerates is 1–3 μm and their diameter is 400–600 nm. The rod-like structures are formed by an ordered assembly of nearly spherical crystallite of about 60 nm in

Table 1: Phase composition, crystallite size, and lattice dimensions of AZO powder synthesized hydrothermally from zinc acetate dehydrate and different Al-precursors and then dried in air at 100°C.

Al-precursor	Phase composition	Quantity (wt%)	Crystallite size (nm) (1 0 1)	(0 0 2)	mean value	a (Å)	c (Å)
Al-chloride	Zincite unidentified peak at $2\theta = 43.27^\circ$	~99 ~1	75 ± 2	77 ± 1	75 ± 3	3.252	5.208
Al-nitrate	Zincite	~99	33 ± 1	62 ± 2	35 ± 1	3.251	5.207
Al-isopropoxide	Zincite	100	30 ± 1	50 ± 2	31 ± 2	3.250	5.206

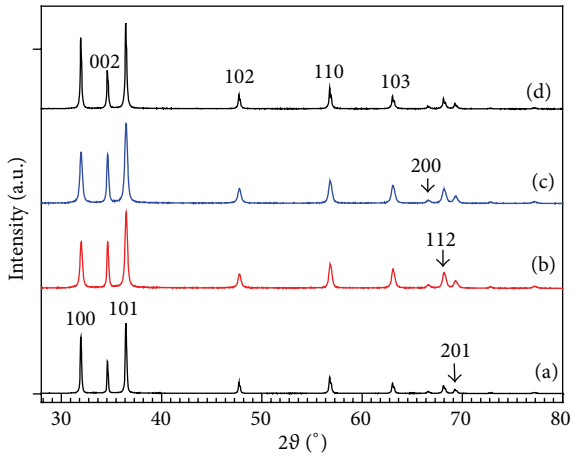

Figure 1: XRD patterns of dried AZO powder prepared from different aluminum precursors, (b) Al-nitrate, (c) Al-isopropoxide, and (d) Al-chloride, all with Al/Zn = 1 mol.%. (a) Pure ZnO. All patterns refer to JCPDS database pdf number 01-070-2551.

size as measured by XRD. On the other hand, the particles obtained using Al-nitrate precursor have irregular aggregated nanoparticles (Figure 2(b)) of size ranges from 1 μm to 4 μm. The agglomerates consist of elongated crystallites with length-to-width ratio of nearly 2 : 1 as detected by XRD. When Al-isopropoxide precursor was used, fine structured nanoparticles free of agglomeration with crystallites size of about 30 nm are formed as depicted in Figure 2(c).

These results indicate that different anions have clear influence not only on particle shape, but also on the particle size. That is because different anions have different properties and are selectively absorbed on the surface of crystal faces to change energy distribution of the surface which in turn affects the growth behavior of these crystals faces, thus changing the morphology.

3.2. Effect of Doping Ratios. AZO nanoparticles based on Al-nitrate precursor, having different Al-doping ratio, namely, Al/Zn molar ratio of 0.5, 1, and 2 mol.%, were investigated in detail. It was chosen among the other samples due to the simple preparation method and low price of starting materials.

3.2.1. Phase and Structural Characterization (XRD). Figure 3 shows XRD patterns of AZO powders synthesised hydrothermally and dried at 100°C for 12 hours, using zinc acetate and Al-nitrate as starting materials with different Al/Zn molar ratios, namely, 0, 0.5, 1, and 2 mol.%. The XRD patterns exhibited extra phases besides the zincite phase. The sample with Al/Zn = 0.5 mol% exhibited zinc oxalate hydroxide ($ZnC_2O_4{\cdot}3Zn(OH)_2$) and hydrozincite ($Zn_5(CO_3)_2(OH)_6$) phases, while in sample with Al/Zn = 1 mol% just traces of a phase with a low peak at $2\theta = 33.40^\circ$ could be detected but could not be identified because of its low intensity. However, the sample with Al/Zn ratio of 2 mol% was free of extra phases rather than zincite phase. Detailed information about the different phases and crystallites parameters of obtained AZO particles with different doping ratios is listed in Table 2.

As seen in Table 2, doping ZnO with aluminum clearly reduces the crystallite size of hydrothermal processed samples. This is because the ionic radius of Al^{3+} (0.535 Å) is smaller than that of Zn^{2+} (0.74 Å) ion which results in a decrease of the unit cell. Further increasing concentration of Al-doping ratio between 0.5 and 2.0 mol.% seems to promote the crystallite growth where the particle size of AZO nanoparticles increased from 15 nm at Al molar ratio of 0.5 mol.% to 47 nm for 2 mol.% (see Figure 4). This seems to be due to exceeding the thermodynamic limit of solubility of Al in ZnO [22], where Al_2O_3 may occur as secondary phase. These results are different from reported data for particle size of AZO films prepared by different deposition methods [23]. The results are in good agreement with the SEM images shown in Figure 7.

Because the ionic radii of Zn^{2+} are larger than those of Al^{3+}, the length of the c-axis is expected to shorten if most of the Al atoms are substituted into Zn sites. Besides the covalent bond length of Al–O is estimated to be shorter than Zn–O. These factors result in a decrease in the volume of the unit cell of AZO. In addition, doping ZnO with Al reduces the zinc interstitials for charge compensation which results in suppressed ZnO grain growth and deteriorated crystallinity. The size effects of aluminum are expected to be seen on the lattice cell which unfortunately does not seem to be really the case at the accuracy of the measurements for a and c axis of the crystal. The position of the (002) zincite peak is expected to shift. Figure 5 shows a slight shift in (002) peak position of the zincite for different Al-doping concentrations in comparison with an undoped zincite powder.

3.2.2. Thermal Analysis. To determine the crystallization conditions, differential thermal analysis (DSC) and TG of AZO nanoparticles (Al/Zn = 1 mol%) dried at 100°C were

Table 2: Phase composition, crystallite size, and lattice parameters of AZO powder synthesized hydrothermally from zinc acetate dehydrate and Al-nitrate with different doping ratio and then dried in air at 100°C.

Doping ratio	Phase composition	Quantity (wt%)	Crystallite size (nm) (1 0 1)	(0 0 2)	mean value	a (Å)	c (Å)
(0%)	Zincite	~90	103 ± 3	195 ± 4	194 ± 4	3.251	5.208
	$ZnC_2O_4 \cdot 3Zn(OH)_2$	~5					
	$Zn_5(CO_3)_2(OH)_6$	~5					
(0.5%)	Zincite	~95	12 ± 1	18 ± 1	15 ± 1	3.249	5.204
	$(Zn_3Al(OH)_8)(NO_3 \cdot 3.04H_2O)$	~5					
(1%)	Zincite	~99	35 ± 1	33 ± 1	35 ± 1	3.251	5.208
	unidentified	~1					
(2%)	Zincite	100	39 ± 2	50 ± 2	47 ± 1	3.250	5.207

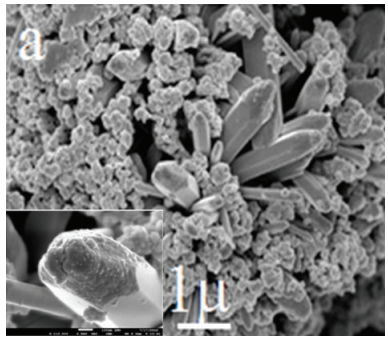

(a)

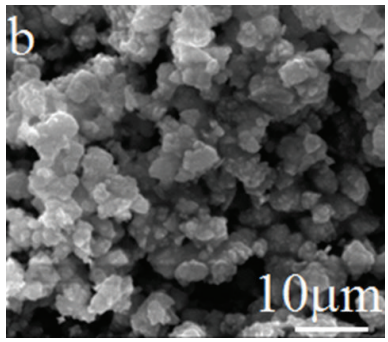

(b)

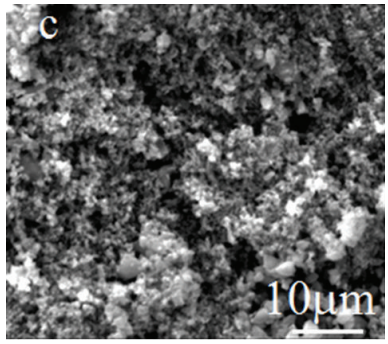

(c)

Figure 2: SEM pictures of AZO particles prepared hydrothermally from the solution of zinc acetate dihydrate and three different Al-precursors: (a) Al-chloride, (b) Al-nitrate, and (c) Al-isopropoxide.

carried out. The specimens were heated from room temperature to 1000°C with an increment of 10°C/min in air. Figure 6 shows a combined plot of DSC and TG. Very small overall weight loss of the nanoparticles is found to take place in the studied temperature range. It is only 1.14% of the initial particles weight. A small endothermic peak is seen in the temperature range of 100°C accompanied by a mass loss of about 0.65% attributed to the evaporation of water from the powder. Very weak broadened peak is noticed in the temperature range of 500°C. It is accompanied by very small weight loss of about 0.23% and is attributed to the burning and consumption of remaining organics. Therefore, the crystallization of AZO nanoparticles occurs at low temperature and it is stable where no phase change is expected to occur at high temperatures.

3.2.3. Metrological Characterization (SEM). Figure 7 shows the SEM morphology of AZO nanopowders with different doping concentration. Remarkable changes in the shape and particles size with the doping ratio are observed. Pure zinc oxide (Figure 7(a)) exhibited large agglomerates with a double head asparagus pack like shaped structure. The agglomerates are formed by an ordered assembly of hexagonal rod-like structures; their lengths ranged from 1 μm to 5 μm and their diameter is of about 800 nm. The incorporation of Al^{3+} into the ZnO seed affected the growth of the host lattice and the nanostructured form. The large agglomerates with asparagus shape seen in pure ZnO disappeared and only hexagonal rod shaped structure is seen. The dimensions of the hexagonal shaped structure differ for different doping ratios where very sharp decrease in the particles size is observed for powder with Al/Zn doping ratio of 0.5 mol%. The particle size is in the range of 10–30 nm. By further increasing the zinc content in the AZO powder, the growth of particle is promoted and its length increased to 30–60 nm for Al/Zn = 1 mol% and 40–70 nm for doping ratio of 2 mol%, which is in agreement with the XRD data in Figure 4.

3.2.4. BET Surface Area. The surface area of AZO nanopowders with different Al/Zn molar ratios was measured. The results showed an increase of the BET surface area of the

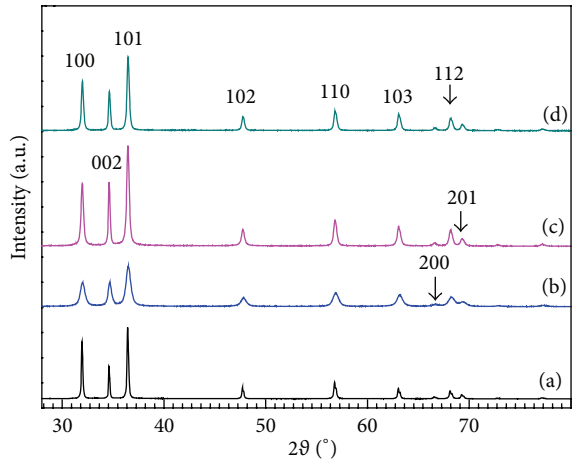

Figure 3: XRD patterns of AZO powders with Al/Zn molar ratio of 0 mol.% (a), 0.5 mol.% (b), 1 mol.% (c), and 2 mol.% (d).

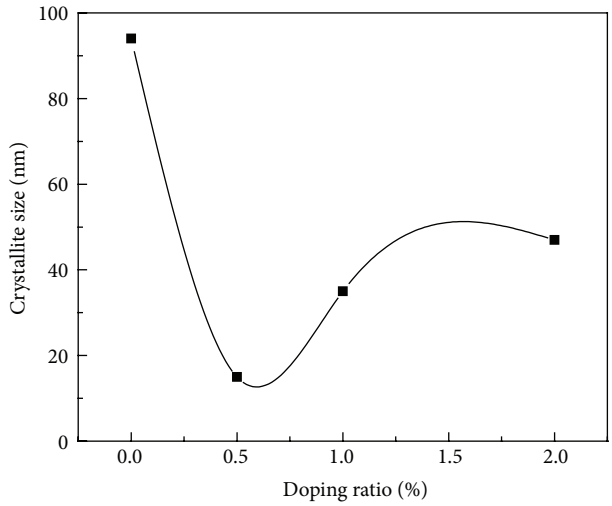

Figure 4: Crystallite size of hydrothermal processed AZO powder with different Zn doping ratio, dried at 100°C, respectively.

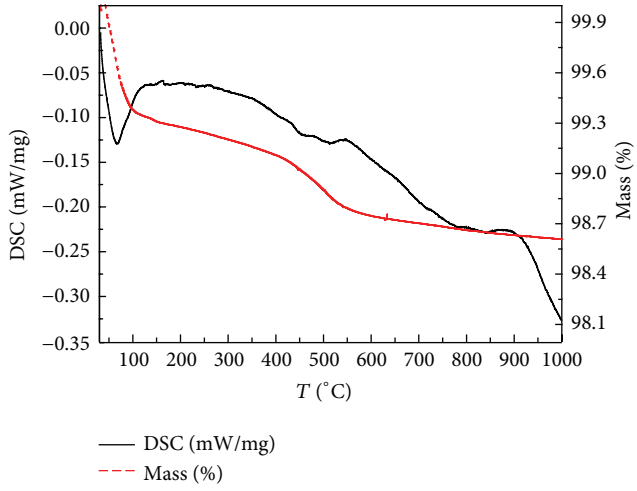

Figure 6: DSC/TG for AZO powder (Al/Zn = 1 mol.%).

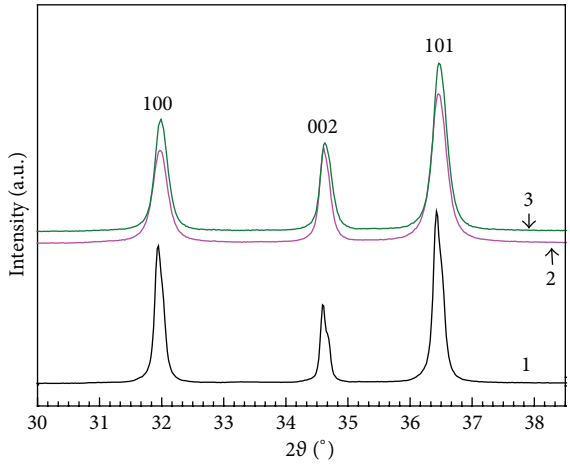

Figure 5: XRD patterns of AZO powders with Al/Zn molar ratio of 0 mol.% (1), 1 mol.% (2), and 2 mol.% (3), respectively.

particles when Al ions are introduced into the ZnO matrix. The BET surface area increased from 6.4 m^2/g for pure ZnO to 20 m^2/g for AZO particles with Al/Zn = 1 mol%. This is consistent with the results of the measurements of the crystallite size calculated from the XRD measurements and the SEM images shown in Figures 4 and 7.

3.2.5. UV/VIS Absorption. The energy gap of the synthesized pure and aluminum doped zinc oxide nanopowders was determined from their UV-VIS absorption spectra. Figure 8(a) shows the absorption spectra of pure ZnO and aluminum doped ZnO measured between 300 and 600 nm. The absorption edge of the spectra is shifted to a higher energy (blue shift) by doping the zinc oxide with aluminum ions, where a reduction of the particle size is observed. The blue shift of the absorption edge can be assigned to the direct transition of electrons in the zinc oxide nanocrystals. The energy band gap (E_g) values can be obtained from the absorption coefficient α, which can be calculated as a function

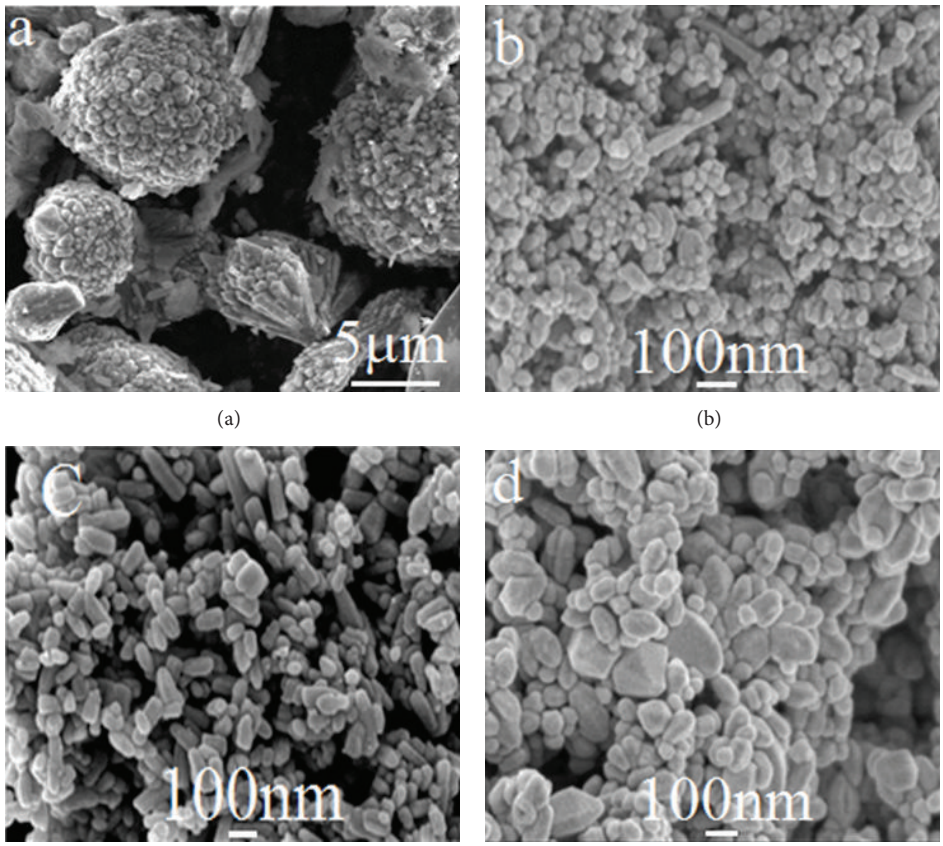

Figure 7: SEM images with different magnifications of AZO nanopowders with different doping ratio: (a) 0, (b) 0.5, (c) 1, and (d) 2 mol.%.

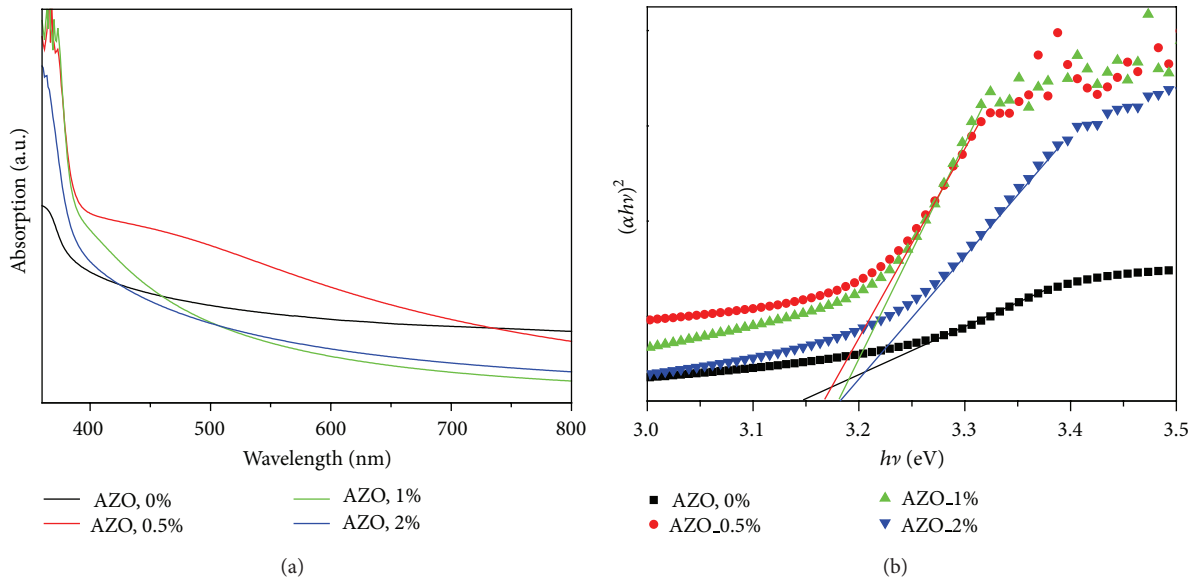

Figure 8: UV/VIS absorption spectrum (a) and $(\alpha h\nu)^2$ versus the photon energy $h\nu$ curve (b) of AZO nanopowders with different doping ratios redispersed in ethanol.

of the photon energy ($h\nu$). The relationship between the absorption coefficient and photon energy can be expressed as [24]

$$(\alpha h\nu)^2 = C\left(h\nu - E_g\right), \quad (1)$$

where C is a constant. α can be calculated from the expression $\alpha = A/d$, where A is the measured absorbance and d is the thickness of the sample in the UV-Vis cell. The E_g value can be obtained by extrapolating the linear portion of the graph of $(\alpha h\nu)^2$ versus $h\nu$, which has been shown in Figure 8(b). The obtained E_g value for pure zinc oxide is 3.15 eV and increased to 3.167 eV for Al-doping ratio of 0.5 mol.% and a further slight increase to 3.185 ev for Al/Zn = 2 mol.%. These values of energy gap are smaller than those of 3.3 eV reported for single crystalline ZnO samples, which may be related to the presence of vacancies and dopants [25]. The blue shift of E_g for AZO nanoparticles was reported by Tarasov and Raccurt [26] and it was attributed to the increase in electron concentration due to Al^{3+} substitution for Zn^{2+}. This effect, known in the literature as the effect of Burstein-Moss, is established as $\Delta E_g \approx n^{2/3}$ [27]. This may be considered as an evidence of the incorporation of Al^{3+} in ZnO lattice [28].

4. Conclusion

Stable AZO nanoparticles have been synthesized using three different Al-precursors using hydrothermal method. XRD measurements showed that obtained particles are crystalline with single zincite phase. Doping ZnO with aluminum reduced the particle size sharply but it starts to increase by further increasing the doping ratio. The powder structure and shape were investigated by SEM and it was found to be influenced strongly by the type of Al-precursor, where it changed from rod-like structure when aluminum chloride was used to nanoparticulate one with aluminum nitrate. The effect of Al-doping ratio on the phase structure, shape, and particle size was also investigated. AZO nanoparticles with a size of 12 nm have obtained for Al/Zn ratio of 0.5 mol.%. By increasing the doping ratio the particle size increased. The specific BET surface area increased with doping ZnO with aluminum. The energy gap is blue-shifted by increasing the doping concentration related to a decrease in the crystallite size. The presence of Al in ZnO was revealed by UV-Vis spectroscopy (a blue shift due to Burstein-Moss effect). DSC/TG analysis showed that the crystallization of AZO nanoparticles occurs at low temperature and no phase change is expected to occur at high temperatures.

Conflict of Interests

The authors declare that there is no conflict of interests regarding the publication of this paper.

Acknowledgments

This work has been financially supported by Leibniz Institute for New Material (INM), Saarbrucken, Germany. A. Alkahlout is thankful to Dr. P. Oliveira for inviting her to join his group as visiting researcher. N. Al-Dahoudi is thankful to DAAD scholarship. The authors thank technicians at INM for their help and support.

References

[1] C. F. Klingshirn, "ZnO: material, physics and applications," *ChemPhysChem*, vol. 8, no. 6, pp. 782–803, 2007.

[2] B. Weintraub, Z. Zhou, Y. Li, and Y. Deng, "Solution synthesis of one-dimensional ZnO nanomaterials and their applications," *Nanoscale*, vol. 2, no. 9, pp. 1573–1587, 2010.

[3] T. P. Chou, Q. Zhang, G. E. Fryxell, and G. Z. Cao, "Hierarchically structured ZnO film for dye-sensitized solar cells with enhanced energy conversion efficiency," *Advanced Materials*, vol. 19, no. 18, pp. 2588–2592, 2007.

[4] P. X. Gao and Z. L. Wang, "Nanoarchitectures of semiconducting and piezoelectric zinc oxide," *Journal of Applied Physics*, vol. 97, no. 4, Article ID 044304, 2005.

[5] S. C. Ko, Y. C. Kim, S. S. Lee, S. H. Choi, and S. R. Kim, "Micromachined piezoelectric membrane acoustic device," *Sensors and Actuators A*, vol. 103, no. 1-2, pp. 130–134, 2003.

[6] S. T. Shishiyanu, T. S. Shishiyanu, and O. I. Lupan, "Sensing characteristics of tin-doped ZnO thin films as NO_2 gas sensor," *Sensors and Actuators B*, vol. 107, no. 1, pp. 379–386, 2005.

[7] M. K. Hossain, S. C. Ghosh, Y. Boontongkong, C. Thanachayanont, and J. Dutta, "Growth of zinc oxide nanowires and nanobelts for gas sensing applications," *Journal of Metastable and Nanocrystalline Materials*, vol. 23, pp. 27–30, 2005.

[8] S. J. Pearton, D. P. Norton, K. Ip, Y. W. Heo, and T. Steiner, "Recent advances in processing of ZnO," *Journal of Vacuum Science and Technology B*, vol. 22, no. 3, pp. 932–948, 2004.

[9] B. Claflin, D. C. Look, S. J. Park, and G. Cantwell, "Persistent n-type photoconductivity in p-type ZnO," *Journal of Crystal Growth*, vol. 287, no. 1, pp. 16–22, 2006.

[10] A. Janotti and C. G. van de Walle, "Native point defects in ZnO," *Physical Review B*, vol. 76, no. 16, Article ID 165202, pp. 1–22, 2007.

[11] A. Janotti and C. G. van de Walle, "New insights into the role of native point defects in ZnO," *Journal of Crystal Growth*, vol. 287, no. 1, pp. 58–65, 2006.

[12] P. Jood, R. J. Mehta, Y. Zhang et al., "Al-doped zinc oxide nanocomposites with enhanced thermoelectric properties," *Nano Letters*, vol. 11, no. 10, pp. 4337–4342, 2011.

[13] A. Favier, D. Muñoz, S. Martín de Nicolás, and P.-J. Ribeyron, "Boron-doped zinc oxide layers grown by metal-organic CVD for silicon heterojunction solar cells applications," *Solar Energy Materials and Solar Cells*, vol. 95, no. 4, pp. 1057–1061, 2011.

[14] V. Bhosle, J. T. Prater, F. Yang, D. Burk, S. R. Forrest, and J. Narayan, "Gallium-doped zinc oxide films as transparent electrodes for organic solar cell applications," *Journal of Applied Physics*, vol. 102, no. 2, Article ID 023501, pp. 1–5, 2007.

[15] P. S. Venkatesh, V. Ramakrishnan, and K. Jeganathan, "Vertically aligned indium doped zinc oxide nanorods for the application of nanostructured anodes by radio frequency magnetron sputtering," *CrystEngComm*, vol. 14, no. 11, pp. 3907–3914, 2012.

[16] J. M. Lin, Y. Z. Zhang, Z. Z. Ye et al., "Nb-doped ZnO transparent conducting films fabricated by pulsed laser deposition," *Applied Surface Science*, vol. 255, no. 13-14, pp. 6460–6463, 2009.

[17] Ü. Özgür, Y. I. Alivov, C. Liu et al., "A comprehensive review of ZnO materials and devices," *Journal of Applied Physics*, vol. 98, no. 4, Article ID 041301, pp. 1–103, 2005.

[18] T. Minami, "Transparent conducting oxide semiconductors for transparent electrodes," *Semiconductor Science and Technology*, vol. 20, no. 4, pp. S35–S44, 2005.

[19] Ç. Kiliç and A. Zunger, "Origins of coexistence of conductivity and transparency in SnO_2," *Physical Review Letters*, vol. 88, no. 9, Article ID 095501, pp. 1–4, 2002.

[20] T. V. Thu and S. Maenosono, "Synthesis of high-quality Al-doped ZnO nanoink," *Journal of Applied Physics*, vol. 107, Article ID 014308, pp. 1–6, 2010.

[21] T. Strachowski, E. Grzanka, W. Lojkowski et al., "Morphology and luminescence properties of zinc oxide nanopowders doped with aluminum ions obtained by hydrothermal and vapor condensation methods," *Journal of Applied Physics*, vol. 102, no. 7, Article ID 073513, pp. 1–9, 2007.

[22] J. G. Lu, Z. Z. Ye, Y. J. Zeng et al., "Structural, optical, and electrical properties of (Zn,Al)O films over a wide range of compositions," *Journal of Applied Physics*, vol. 100, no. 7, Article ID 073714, 2006.

[23] H.-M. Zhou, D.-Q. Yi, Z.-M. Yu, L.-R. Xiao, and J. Li, "Preparation of aluminum doped zinc oxide films and the study of their microstructure, electrical and optical properties," *Thin Solid Films*, vol. 515, no. 17, pp. 6909–6914, 2007.

[24] S. Maensiri, P. Laokul, and V. Promarak, "Synthesis and optical properties of nanocrystalline ZnO powders by a simple method using zinc acetate dihydrate and poly(vinyl pyrrolidone)," *Journal of Crystal Growth*, vol. 289, no. 1, pp. 102–106, 2006.

[25] X. C. Wang, X. M. Chen, and B. H. Yang, "Microstructure and optical properties of polycrystalline ZnO films sputtered under different oxygen flow rates," *Journal of Alloys and Compounds*, vol. 488, no. 1, pp. 232–237, 2009.

[26] K. Tarasov and O. Raccurt, "A wet chemical preparation of transparent conducting thin films of Al-doped ZnO nanoparticles," *Journal of Nanoparticle Research*, vol. 13, no. 12, pp. 6717–6724, 2011.

[27] P. K. Basu, *Theory of Optical Processes in Semiconductors: Bulk and Microstructures*, Oxford University Press, New York, NY, USA, 1997.

[28] P. Kadam, C. Agashe, and S. Mahamuni, "Al-doped ZnO nanocrystals," *Journal of Applied Physics*, vol. 104, no. 10, Article ID 103501, 2008.